Al-Doped Octahedral Cu2O Nanocrystal for Electrocatalytic CO2 Reduction to Produce Ethylene

Sanxiu LI , Xuelan Sha , Xiafei Gao , Juan Peng *

Posted Date: 11 July 2023

doi: 10.20944/preprints202307.0713.v1

Keywords: electrocatalysis; electronic structure; Faradaic efficiency; ethylene

Article

Al-Doped Octahedral Cu_2O Nanocrystal for Electrocatalytic CO_2 Reduction to Produce Ethylene

Sanxiu Li †, Xuelan Sha †, Xiafei Gao and Juan Peng *

State Key Laboratory of High−Efficiency Utilization of Coal and Green Chemical Engineering, College of Chemistry and Chemical Engineering, Ningxia University, Yinchuan 750021, China

* Correspondence: pengjuan@nxu.edu.cn

† These authors contributed equally to this work.

Abstract: Ethylene is an ideal CO_2 product in an electrocatalytic CO_2 reduction reaction (CO_2RR), which has high economic value. In this paper, Al–doped octahedral Cu_2O (Al–Cu_2O) catalyst was synthesized by a simple wet chemical method. The selectivity of CO_2RR products was improved by doping Al onto the surface of octahedral Cu_2O by regulating the Al content. The Al–Cu_2O was used as an efficient electrocatalyst for CO_2RR with selective ethylene production. The Al–Cu_2O exhibited a high Faradic efficiency (FE_{C2H4}) of 44.9% at -1.23 V (vs. RHE) in CO_2 saturated 0.1 M $KHCO_3$ electrolyte. Charge transferring from Al atom to Cu atom take place after Al doping in Cu_2O, thereby optimizing the electronic structure, which facilitates CO_2RR to ethylene production. The DFT calculation showed that the Al–Cu_2O catalyst can effectively reduce the adsorption energy of the *CHCOH intermediate and promote the mass transfer of charges, thus improving the FE_{C2H4}. After Al doping into Cu_2O, the center of d orbitals shift positively, which makes the d–band closer to the Fermi level. Furthermore, the density of electronic states increases, which was conducted to the interaction between Cu atoms and intermediates, thus accelerating the electrochemical CO_2 reduction process. This work proved that the metal doping strategy can effectively improve the catalytic properties of Cu_2O, thus providing a useful way for CO_2 cycling and green production of C_2H_4.

Keywords: electrocatalysis; electronic structure; faradaic efficiency; ethylene

1. Introduction

The increased CO_2 emissions in atmosphere results in serious greenhouse effect and the elevated sea level [1,2]. The electrochemical CO_2 reduction reaction (CO_2RR) is a promising strategy to mitigate the global warming and energy crisis, while transforming CO_2 into fules and chemical feedstocks [3, 4, 5]. It can use clean electric energy generated by renewable solar and wind energy to drive the conversion of CO_2 under mild conditions [6, 7]. The reduction products of CO_2RR include CO [8–10], HCOOH [11–14], alcohols [15–17], and various hydrocarbons [18–20]. Among them, C_2H_4 has attracted more and more attention due to its high energy density. Furthermore, C_2H_4 is regarded as an important component in the production of various plastics, solvents, and cosmetics in the chemical industry [21].

Up to now, Cu-based materials can electrocatalytic convert CO_2 into C2/C2+ products. Among reported Cu-based catalysts, Cu_2O nanocrystal has attracted much attention due to their electrocatalytic activity and high selectivity toward C_2H_4. To improve the CO_2RR performance of Cu_2O, great efforts have been made on its structural design. Metal ions can be used as structure-guiding agents to optimize the micro-structure of nanocrystals [22].Cu_2O nanoparticles (Cu_2O NPs) exhibit good performance for CO_2RR, possibly because the low coordination Cu^+ on the surface contributes to C-C coupling, thus promoting the production of C_2H_4 [23]. Other strategies including crystal facet controlling [24], defect engineering [25,26], alloying [27], valence adjustment [28], and surface molecular modification [29] have been employed to improve the electrocatalytic performance

 doi:10.20944/preprints202307.0713.v1

of CO_2RR to produce C_2H_4. For example, Shang et al. [30] have designed a core-shell Cu@Cu_2O catalyst, on which a thin layer of natural oxide grows on the surface under environmental conditions. The synergistic effect between Cu^+ and Cu^0 on the Cu@Cu_2O surface helps to improve its efficiency and selectivity for C2 products. Ning et al. [31] reported the preparation of Cu_2O/nitrogen-doped carbon shell (Cu_2O/NCS) composite and its application in CO_2 electroreduction to selective formation of C_2H_4. However, copper catalysts still face many problems, such as inevitable competitive hydrogen evolution reaction, complex reaction mechanisms diversification of products, and low selectivity of target products [32] Therefore, it is of huge challenge to design CO_2RR electrocatalysts with high activity, selectivity and satisfied stability.

In this work, an effective strategy was proposed to improve the CO_2RR product by doping Al on the surface of octahedron Cu_2O nanocrystals. Al doped Cu_2O (Al–Cu_2O) was used as an effective electrocatalyst for selective ethylene production by CO_2RR. Al–Cu_2O exhibits a high Faraday efficiency (FE_{C2H4}) of 44.9% at -1.23 V (vs. RHE). During the coupling process of * CHCOH intermediate, the Al–Cu_2O catalyst can significantly reduce the free energy and promote the formation of C_2H_4. It can also inhibit the occurrence of HER side reaction. Therefore, the doping strategy is beneficial for the adsorption of intermediates to reconstruct the internal stable state of electronic structure of Cu_2O, thus improving the activity and selectivity of CO_2 conversion to ethylene.

2. Results

2.1. Morphology and structure analysis

As shown in Figure 1, Al–Cu_2O–X catalyst was prepared by a simple one-step method (Experimental section for details). In order to further characterize Al–Cu_2O–X catalysts, XRD pattern was used to study the crystal structure of Cu_2O, Al–Cu_2O, and Al–Cu_2O–2. From the XRD pattern in Figure 2a, the peaks at 29°, 36°, 42°, 61°, 73°, and 77° correspond to the (110), (111), (200), (220), (311) ,and (222) planes of Cu_2O, respectively, which agree well with the octahedral Cu_2O (PDF#75–1535). The XRD patterns of Al–Cu_2O–X (3-6) were shown in Figure S1. During the preparation process, the catalyst synthesized by adjusting the amount of Al^{3+}, the concentration of NaOH, and the reaction time. Al–Cu_2O–X (3-6) were all single-phase Cu_2O nanocrystals. The morphologies of the Cu_2O, Al–Cu_2O, and Al–Cu_2O–2 were monitored by scanning electron microscopy (SEM). Cu_2O nanocrystal without Al doping showed a octahedron shape with smooth surface (Figure S2a). Due to the doping effect of Al, the Al–Cu_2O nanocrystal presented a octahedral shape with a more rough surface and formed a defect structure (Figure 2b), which may provide abundant active sites for CO_2RR [33]. When the concentration of Al^{3+} increased from 0.02 M to 0.03 M, Al–Cu_2O–2 catalyst exhibits a cube shape (Figure S2b). However, it was reported that the resulting cube Al–Cu_2O catalyst is not conducive to the formation of C_2H_4 [23]. The better-performing Al-Cu_2O with a homo-octahedral shape was observed by TEM (Figure 2c), which was consistent with SEM image. High resolution transmission electron microscopy (HRTEM) image in Figure 2d presented that the lattice stripe spacing d marked was 0.304 nm, corresponding to the (110) crystal plane of Cu_2O. The HAADF-STEM image (Figure 2e) also exhibited an octahedral shape. The composition of Al-Cu_2O was reconfirmed by elemental mapping (Figure 2f). The Al (red), Cu (blue), and O (green) elements uniformly distributed over the Al-Cu_2O nanocrystals.

Preprints (www.preprints.org) | NOT PEER-REVIEWED | Posted: 11 July 2023 doi:10.20944/preprints202307.0713.v1

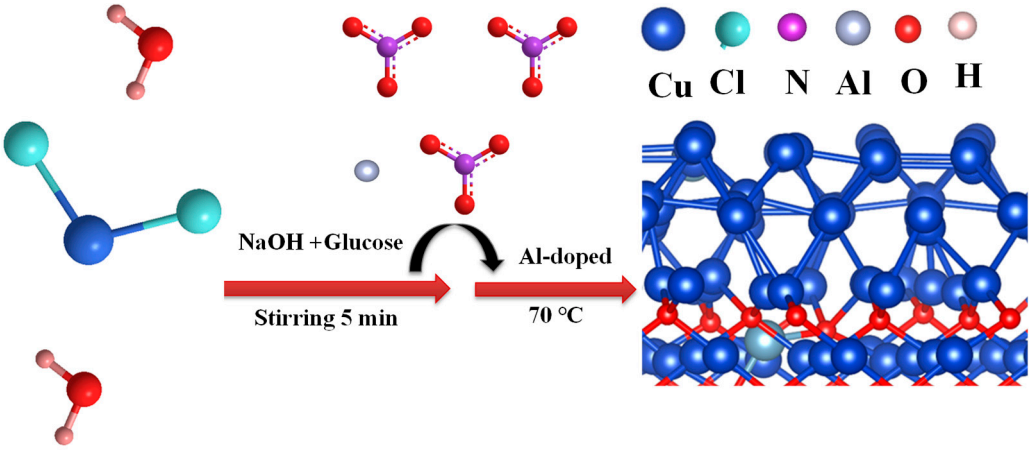

Figure 1. Schematic illustration of the fabrication process for Al–Cu_2O–X (X=2、3、4、5、6).

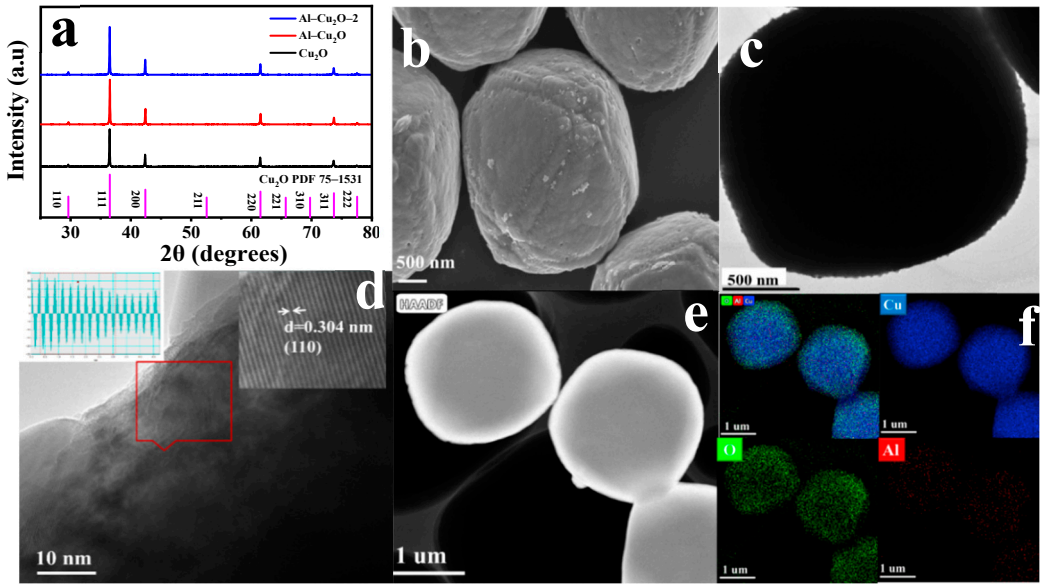

Figure 2. Characterization of Al–Cu_2O: (a) XRD, (b) SEM, (c) TEM, (d) HRTEM, (e) HAADF–TEM, and (f) elemental mapping (blue, green and red represents Cu, O and Al element, respectively).

The surface composition and valence of Cu_2O and Al–Cu_2O nanoscrystals were characterized by X-ray photoelectron spectroscopy (XPS). As shown in Figure 3a and b, four peaks were observed in Cu 2p spectrum for both Cu_2O and Al–Cu_2O samples. For Cu_2O, the peaks at 932.78 and 952.62 eV corresponded to the binding energies of Cu $2p_{3/2}$ and Cu $2p_{1/2}$ of Cu_2O or Cu, respectively. The binding energies at 935.28 eV and 944.48 eV were ascribed to the peaks of Cu^{2+}. For Al–Cu_2O, the peaks at 932.89 and 952.73 eV corresponded to the Cu $2p_{3/2}$ and Cu2 $p_{1/2}$ of Cu_2O or Cu, respectively. The binding energy of 935.26 and 944.46 eV belonged to the peak of Cu^{2+}. The above results showed that the existence of Cu^0 may be due to the partial reduction of Cu_2O in the CO_2RR process [34]. The existence of trace CuO may be mainly due to the oxidation of a small amount of Cu_2O catalyst to CuO in the air after the synthesis of Cu_2O [35]. When octahedral Cu_2O nanocrystals were doped with Al, the peaks of Cu $2p_{3/2}$, Cu $2p_{1/2}$, and Cu^{2+} of Cu_2O or Cu were shifted positively. This results may be attributed the introduction of Al, which can induce charge transfer from Al atoms to Cu atoms, thus modulating the electronic structure of Al–Cu_2O. The existence of Cu_2O was also confirmed in the O 1s XPS spectra of Cu_2O and Al-Cu_2O (figure 3c-d). There were three XPS peaks in both catalysts, of which the peak at 530.5 eV corresponds to the Cu-O bond, and 532.11 and 532.77 eV correspond to

Preprints (www.preprints.org) | NOT PEER-REVIEWED | Posted: 11 July 2023 doi:10.20944/preprints202307.0713.v1

Olat and C=O, respectively [36]. In the high-resolution spectrum of Al 2p (figure 3e), the peaks at 74.55 and 77.35 eV correspond to the Al $2p_{1/2}$ and Al $2p_{3/2}$ of metal Al, respectively. The Al atom was 0.41% by XPS analysis, indicating that the Al–Cu_2O catalyst has been successfully prepared.

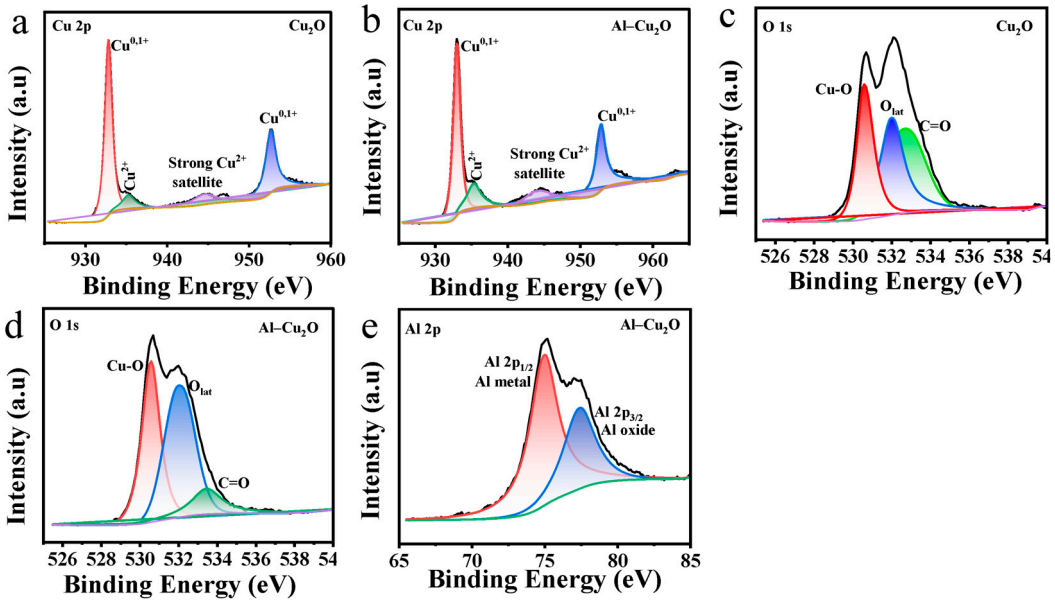

Figure 3. XPS spectrum of Cu 2p: (a) Cu_2O and (b)Al–Cu_2O, O 1s spectrum of (c) Cu_2O and (d) Al–Cu_2O, (e) Al 2p spectrum of the Al–Cu_2O.

2.2. Electrocatalytic CO_2RR perfomances

To further analyze the electrochemical performance of the catalyst, the linear sweep voltammetry (LSV) of Cu_2O and Al–Cu_2O–X catalysts in saturated CO_2 electrolyte and saturated N_2 electrolyte were tested. The analysis of Figure 4a shown that the current density of Al–Cu_2O catalyst in CO_2 saturated electrolyte is higher than that in N_2, indicating that Al–Cu_2O catalyst had higher activity. The LSV curve was measured in CO2-saturated 0.1 M $KHCO_3$ electrolyte (figure S3a). The current density of the Al–Cu_2O catalyst in CO_2 saturated atmosphere was higher than that of Cu_2O and Al–Cu_2O–2 catalysts, indicating that the Al–Cu_2O catalyst had better electrocatalytic activity for CO_2RR. Figure S3b shows the potentiostatic electrolysis of CO_2 at various potentials. The almost constant current signal indicates that the Al-Cu_2O catalyst exhibited good electrochemical stability during the CO_2RR process. In Figure 4b, the formation rates of three kinds of catalysts were presented for ethylene products. The Al–Cu_2O catalyst has higher current density for ethylene formation than that of Cu_2O and the Al–Cu_2O–2 catalysts in a wide potential range, and reaches the partial current density of 16.7 mA cm^{-2} at -1.38 V (vs. RHE). The above results showd that the Al–Cu_2O catalyst was more conducive to the production of ethylene as the main product and has a better inhibitory effect on compete hydrogen formation.

In order to determine the CO_2RR selectivity of the Al–Cu_2O catalyst, the reduction products were qualitatively and quantitatively analyzed. In this study, the reduction products of each catalyst were determined in the wide potential range from-0.98 V to-1.38 V (vs. RHE). The analysis of Figure 4c and S4 shows that the products of Cu_2O ,and Al–Cu_2O–X catalysts were C_2H_4, $HCOO^-$, CO, CH_4 and by-product H_2. When Al^{3+} was not introduced in the reaction, the octahedral Cu_2O nanocrystal catalyst was synthesized, and Figure S4a shows the FE of the catalyst to the CO_2RR product. The result shown that the catalyst had a good effect on inhibiting by product H_2 at low potential, and the highest FE_{C2H4} was 26.1%. If an appropriate amount of Al^{3+} was introduced into octahedral Cu_2O nanocrystal (0.02 M), the selectivity of Al–Cu_2O catalyst was improved. As shown in Figure 4b, with the increase of catalyst potential, the FE value of H_2 decreases from 35.1% to 22.1%. On the contrary, the FE value of C_2H_4 increases from 12.9% at-0.98 V (vs. RHE) to 44.9% at-1.23 V (vs. RHE). The result shown that the

 doi:10.20944/preprints202307.0713.v1

catalyst had good selectivity for ethylene and good inhibition effect on HER. If more Al^{3+} was added to the reaction (0.03 M), the FE of the prepared Al–Cu_2O–2 catalyst for the CO_2RR product was shown in Figure S4b. The result has shown that the FE of C_2H_4 was 32.8%, indicating that the catalyst had a good selectivity for ethylene. It was worth noting that we also studied the effects of reaction time (S4cpender d) and NaOH concentration (S4ePowerf) on the selectivity of the catalyst. The result showed that the FE of the four catalysts C_2H_4 was 40.1%, 38.6%, 41.0%,and 30.8%, respectively, indicating that the optimization of reaction time and NaOH concentration can make the catalyst have a certain selectivity, but compared with the quantity conditions of introducing Al^{3+}. The effect of improving the selectivity of the product is weaker, mainly because the addition of different amounts of Al^{3+} will form different morphology of the catalyst, resulting in different selectivity of the catalyst to the product. Figure 4d compares the selectivity of three kinds of catalysts Cu_2O, Al–Cu_2O, and Al–Cu_2O–2 for ethylene products. The result showed that under different applied voltages, the efficiency of the Al–Cu_2O catalyst for reducing CO_2 to C_2H_4 in 0.1 M $KHCO_3$ electrolyte was higher than that of the other two catalysts, indicating that the amount of Al^{3+} introduced into the catalyst effected the selectivity of the catalyst. This may be due to the fact that Al -doped Cu_2O will cause changes in the electronic structure and the morphology of the catalyst, thus reducing the adsorption energy of the catalyst for ethylene intermediates in the CO_2RR process and enhancing the selectivity of the reaction to the products.

The electrochemical surface area (ECSA) is also a key point for the electrocatalyst. According to the formula for calculating ECSA, it is known that this parameter is related to the C_{dl} and C_{ds} values of their catalysts, because the catalysts are coated on hydrophobic carbon paper (model 060). Therefore, the Cds of the three catalysts are the same, and only the C_{dl} value of the catalyst can be calculated to determine the ECSA of the catalyst. According to the Cu_2O, Al–Cu_2O, and Al–Cu_2O–2 catalysts, the cyclic voltammograms (Figure S5a-c) of 0.47 V~0.57 V (vs. RHE) at different scanning rates (20, 40, 60, 80,100, 120 mV s^{-1}). It can be seen from Figure 4e that the capacitance values of Cu_2O, Al–Cu_2O, and Al–Cu_2O–2 catalysts were 0.109, 0.122, and 0.076 mF cm^{-2}, respectively. The largest C_{dl} of the Al–Cu_2O electrocatalyst suggested that the high electrochemical activity surface area of the Al–Cu_2O–2 catalyst. This high ECSA can offer a lot of catalytic active sites for improving the electrocatalytic performance of CO_2RR, thus improving the selectivity of the catalyst, which was consistent with the previous research conclusion.

The impedance of several different catalysts under open-circuit voltage was obtained (Figure S6a). Compared with the octahedral Cu_2O catalyst without Al doping, the EIS arc of the Al–Cu_2O catalyst was smaller than that of the octahedral Al–Cu_2O catalyst. The results indicate that during the reaction process, interface charges can be rapidly transferred and catalytic activity can be improved. In order to better understand the activity and kinetics of Al-Cu_2O materials on CO_2RR, the Tafel slope analysis of the local current density of the catalyst product is carried out. As shown in Figure 4f, the Tafel slope of the Al–Cu_2O catalyst (74.3 mV dec^{-1}) was lower than that of Cu_2O (85.9 mV dec^{-1}) and the Al–Cu_2O–2 (110.4 mV dec^{-1}), indicating that the electron transfer rate of the catalyst is faster, which was beneficial to the rapid adsorption and desorption of the important intermediate of ethylene from the surface of Al–Cu_2O catalyst. To speed up the reaction, therefore, the introduction of Al into octahedral Cu_2O catalyst may help to reduce the activation energy of various intermediates in the CO_2RR reaction process, thus making the catalyst show better selectivity and activity for the products.

Preprints (www.preprints.org) | NOT PEER-REVIEWED | Posted: 11 July 2023 doi:10.20944/preprints202307.0713.v1

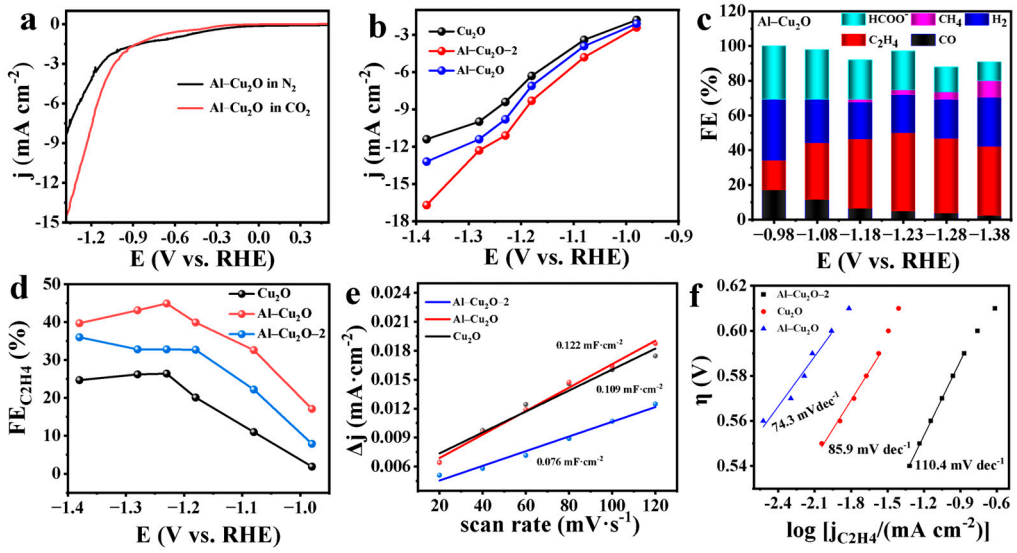

Figure 4. (a) the polarization curves of Cu_2O, Al–Cu_2O and Al–Cu_2O–2 catalysts in 0.1 M $KHCO_3$ aqueous solutions with saturated CO_2, (b) partial current density of Cu_2O, Al–Cu_2O and Al–Cu_2O–2 catalysts, sweeping speed of 5 mV s^{-1}, (c) FE values of Al-Cu_2O catalyst in 0.1 M $KHCO_3$ aqueous solutions with saturated CO_2, (d) The FE_{C2H4} values of Cu_2O, Al–Cu_2O and Al–Cu_2O–2 catalysts, (e) The linear relationship between △J and scanning rates , (f) Tafel plots of Cu_2O, Al–Cu_2O and Al-Cu_2O–2.

We further studied the stability of the CO_2RR material. As seen in Figure 5a, the Al–Cu_2O catalyst was electrolyzed at-1.23V (vs. RHE) for about 25000s. The analysis chart shown that the current density of the Al–Cu_2O catalyst can be kept stable and the FE of ethylene can be kept above 40% in the first 3600s. With the change in reaction time, the current density increases gradually. By observing the stable SEM of the Al–Cu_2O catalyst, we can see that there are some small pores on the surface of the catalyst, which may provide more active sites, thus increasing the current density. However, the selectivity of the catalyst to ethylene, the main product, began to decrease obviously after two hours of testing, probably because the catalyst was dripped on hydrophobic carbon paper during the test, which may lead to the shedding of the catalyst in the long-term electrolysis process, resulting in a decrease in the FE of the catalyst. At the same time, in the current research, the stability of copper-based catalysts is poor, in later research, other strategies need to be used to improve the stability of copper-based catalysts for a long time [37]. Through the XRD spectrum after long-term electrolysis, it was found that the composition of the electrode was consistent with that before the reaction, indicating that the Al–Cu_2O showed good electrochemical stability (Figure 5b) in the whole CO_2RR test. It was worth noting that after the electrolysis of Al–Cu_2O catalyst for 10min, 20min, 30min and 7h (Figure S7a-d), the result showed that the morphology of the octahedron remains unchanged. With the increase of electrolysis time, some small pores appear on the surface of the catalyst. The appearance of these pores may provide more active sites, resulting in an increase in current density in the electrolysis process, but a decrease in the FE of ethylene. The result shown that the increase of these active sites was not conducive to improving the selectivity of the main products, and the above results shown that the catalyst can maintain good stability under long-term electrolysis.

Preprints (www.preprints.org) | NOT PEER-REVIEWED | Posted: 11 July 2023 doi:10.20944/preprints202307.0713.v1

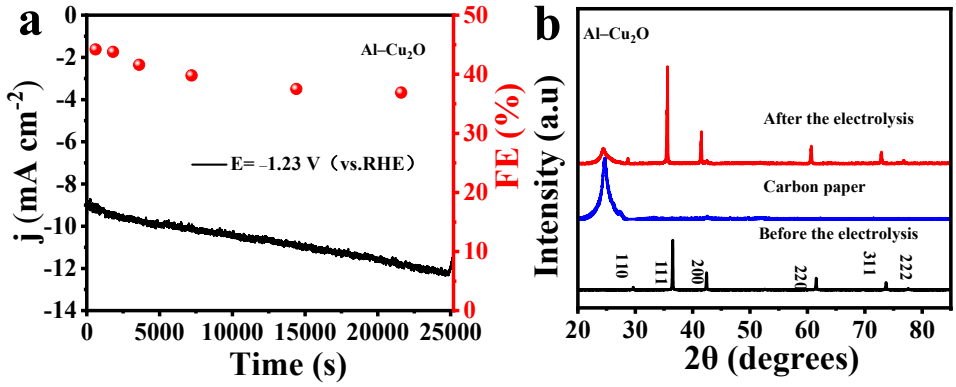

Figure 5. Al–Cu_2O catalyst in 0.1 M $KHCO_3$ electrolyte (a) electrochemical stability test pattern and (b) the XRD of Al–Cu_2O catalyst after long–term stability test.

2.3. DFT Computations

In order to further explore the catalytic reaction mechanism, we used Density functional theory (DFT) to calculate, simulate and compare the CO_2RR reaction path on the surface of Al-Cu_2O and Cu_2O catalysts to further understand the path from CO_2 to C_2H_4. Figure 6 shows the spatial structure (Figure 6a) and energy distribution of Al–Cu_2O and Cu_2O. Figure 6b shown the energy distribution of ethylene production and by-product H_2 of Cu_2O and Al–Cu_2O catalysts. The Gibbs free energies of each intermediate along ethylene on Cu_2O and Al-Cu_2O catalysts *CHCOH, *CCH, *CCH, *CCH_2, *$CHCH_2$ (intermediates for ethylene production) and *H (intermediates to H_2) have been calculated. Because the Gibbs free energy of Al–Cu_2O catalyst was lower than that of Cu_2O catalyst in each reaction step, the path of ethylene production of CO_2RR was easier to occur. It can be seen that the strategy of doping Al to octahedral Cu_2O was beneficial to improve the selectivity of product C_2H_4 [38]. At the same time, the analysis of figure 6c shows that the Al-Cu_2O catalyst doped with Al enhances the adsorption of intermediate * H and was further away from the ideal hydrogen adsorption value (0 eV). It makes the competitive reaction of HER more disadvantageous, thus inhibiting the occurrence of side effects.To further analyze the potential reason for the selective improvement of this product, the density of states (DOS) of d orbitals on Cu_2O (001) and the Al–Cu_2O (001) surfaces before CHCOH adsorption is compared (Figure 6d,e). Since the electronic states near the Fermi level are mainly contributed by the d electrons of Cu atoms, it is indicated that the reaction is mainly caused by the interaction between Cu and C, and the d band center of undoped Al octahedron Cu_2O (001) was -2.08 7eV. The d-2.027 eV of the Al-doped Al–Cu_2O (001) surface was closer to the Fermi level (0eV), and the d-band shifts upward on the Abscissa, which makes the center of the d-band closer to the Fermi level and increases the density of electronic states, which is beneficial to the adsorption of Cu atoms through d electrons and intermediates, thus promoting the CO_2RR process and improving the selectivity of the catalyst for C_2H_4 product.

Preprints (www.preprints.org) | NOT PEER-REVIEWED | Posted: 11 July 2023 doi:10.20944/preprints202307.0713.v1

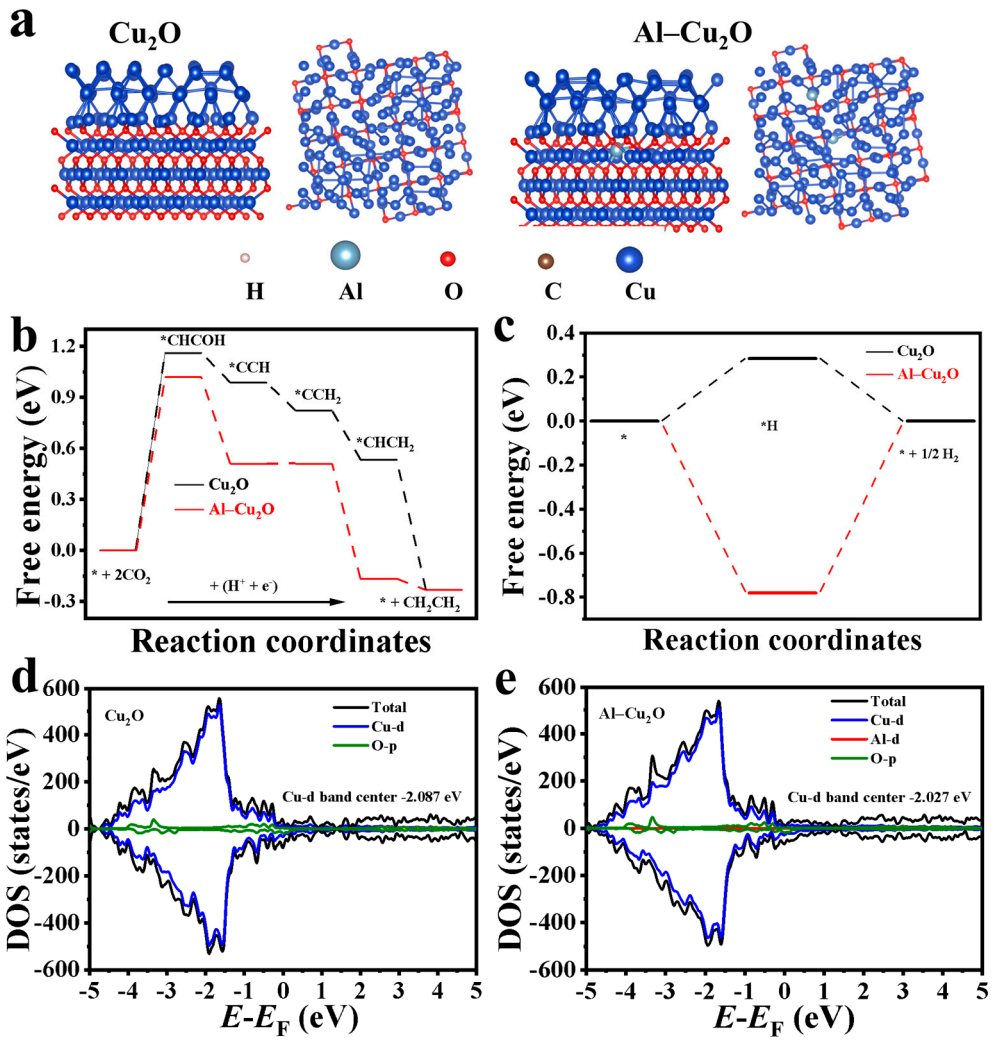

Figure 6. Free energy diagram of ethylene and hydrogen produced by CO_2RR on the surface of (a) side and top views of Cu_2O (001) and Al–Cu_2O (001) configurations, (b) Cu_2O (001) and (c) Al-Cu_2O (001) catalysts, DOS of d orbitals on (d) Cu_2O (001) and (e) Al–Cu_2O (001) surfaces before *CHCOH adsorption.

3. Materials and Methods

3.1. Preparation of Al-Cu2O nanocrystals

The Al-Cu_2O nanocrystals was synthesized with a improved method according to the literature [39]. The specific step was as follows: 10 mL of 0.6 M NaOH aqueous solution was first added to the sample bottle. Subsequently, $CuCl_2·2H_2O$、$Al(NO_3)_3·9H_2O$ and glucose were added to the sample bottle successively. The concentrations of $CuCl_2·2H_2O$, $Al(NO_3)_3·9H_2O$,and glucose in the solution were 0.10 M, 0.02 M, and 0.07 M, respectively. After continuous agitation for 5min, the sample bottle was placed in a 70℃ water bath and vigorously stirred for 4min. The precipitation obtained by centrifugal collection was rinsed with deionized water, and finally dried under vacuum at room temperature for 12 h to obtain Al–Cu_2O catalyst. At the same time, the effects of the amount of Al^{3+}, the concentration of NaOH and the reaction time on ethylene products were also investigated in this chapter, and the optimum preparation conditions were obtained, as shown in the following table S1-1.

Preprints (www.preprints.org) | NOT PEER-REVIEWED | Posted: 11 July 2023 doi:10.20944/preprints202307.0713.v1

3.2. Preparation of Al-Cu_2O coated carbon paper electrode

5 mg of the prepared catalyst was taken and added to 25 μL of Nafion, followed by 300 μL of distilled water and 175 μL of ethanol to prepare 500 μL of reagent, which was mixed by sonication for 2 hours and then 100 μL was uniformly applied with a pipette to a carbon paper type 060 with a total surface area of 1 cm^2. The loading on the carbon paper was calculated to be 1 mg cm^{-2} and subsequently dried in a vacuum oven to obtain the Al-Cu_2O electrode for the next test.

3.3. Electrochemical measurements

The electrocatalytic CO_2RR was carried out in an H-type electrolytic cell with a proton exchange membrane (Nafion 117) separating the electrolyte. Working electrodes were prepared, with a platinum sheet (1 cm^2) as the counter electrode and Ag/AgCl (saturated KCl) as the reference electrode. Before conducting the experimental test, CO_2 (99.999% purity) or N_2 gas was introduced into the electrolytic cell, which was saturated with 0.1 M $KHCO_3$ (pH=6.8) electrolyte after approximately 30 min. In this work, all electrochemical performance was measured on the electrochemical workstation (CHI760E, Shanghai Chenhua). Convert all electrode potentials into electrode potentials relative to RHE through Nernst equation: $\mathrm{E\,(vs.\,RHE)} = \mathrm{E\,(vs.\,Ag/AgCl)} + 0.0591 \times \mathrm{pH} + 0.197$ V. The electrochemical active surface area was tested by the cyclic voltammetry curves of the bilayer capacitance values at different scanning rates (20, 40, 60, 80, 100 and 120 mV s^{-1}). The gaseous products were collected by electrolysis of the four catalysts in a 0.1 M $KHCO_3$ electrolyte saturated with CO_2 for 10 min at different measurement potentials and then analyzed by using gas chromatography (8890, Agilent). The liquid products of the four catalysts were collected by electrolysis in an aqueous 0.1 M $KHCO_3$ solution saturated with CO_2 for 30 min at each measurement potential, followed by qualitative and quantitative analysis using ion chromatography (AS-DV, Thermo Scientific, America).

3.4. Product analysis

The gas products are detected by gas chromatography (GC, Agilent 8890) directly from the gas outlet. The carbonaceous gas products from the cathode chamber are analyzed by a methane reformer and flame ionization detector (FID). A thermal conductivity detector (TCD) was used to detect the eCO_2RR by-product H_2. When the current stabilizes, the gas product is detected. Quantification of the gaseous products was determined by comparison with the standard curve. the Faraday efficiency (FE) of C_2H_4, H_2 and CO was calculated as follows:

$$\mathrm{FE} = \frac{N \times n \times v \times F}{V_m \times j} \times 100\%$$

where v is the CO_2 flow rate (v= 20 mL min^{-1}), n is the total molar fraction of C_2H_4, H_2 or CO of the gas measured in the GC, N is the number of electrons required to form a molecule of H_2 or CO (N=2), F is Faraday's constant (96485 C mol^{-1}), and V_m is the molar volume of the gas at 298 K and j is current at each potential (A).

Liquid products Faraday efficiency test method:A saturated solution of electrocatalytic CO_2 was electrocatalyzed by the Coulomb method using a controlled potential, and the electrolytic reduction product was analyzed and calculated after 0.5 h. The CO_2 flow rate during electrolysis was controlled at 20 mL min^{-1} and the liquid product was determined by ion chromatography (AS-DV, Thermo Scientific, America). The FE of the liquid phase product was calculated as follows:

$$\mathrm{FE} = \frac{NnF}{Q} \times 100\%$$

where N is the number of electrons transferred, n is the amount of formate in the cathode chamber, F is Faraday's constant (96485 C mol^{-1}) and Q is the total charge passing through the electrode.

4. Conclusions

In summary, the Al-doped octahedral Cu_2O nanocrystal was successfully prepared and used as an efficient CO_2RR electrocatalyst. The Al–Cu_2O exhibited high activity and selectivity for ethylene

production. The Al–Cu_2O catalyst demonstrate a high faradaic efficiency 44.9% at -1.23V (vs. RHE) for C_2H_4 production. The high catalytic activity for CO_2 electrochemical reduction is due to optimized electronic state by Al doping in octahedral Cu_2O nanocrystal. The DFT simulation suggested the C–C coupling mechanism, and proved that the catalyst Al–Cu_2O doped Cu_2O octahedron can greatly reduce the free energy in the coupling process of *CHCOH intermediate, promote the formation of C_2H_4, and inhibit the occurrence of HER side effect. Therefore, the active degree of electronic states increases, which was conducive to the adsorption of Cu atoms and intermediates, improving the selectivity of product C_2H_4. Furthermore, our work demonstrates a simple doping strategy for the preparation of novel copper-based catalysts, which can be extended to the design and study of other types of highly efficient electrocatalysts.

Acknowledgments: This work was financially supported by the National Natural Science Foundation of China (No. 22262027). We also acknowledged the support of Ningxia leading scientific and technological innovation talents projects (No.KJT2018002), and Ningxia Natural Science Foundation (No.2022AAC03103).

Conflicts of Interest: The authors declared that there was no competing financial interest.

References

1. Alli, Y. A.; Oladoye, P. O.; Ejeromedoghene, O.; Bankole, O. M.; Alimi, O. A.; Omotola, E. O.; Olanrewaju, C. A.; Philippot, K.; Adeleye, A. S.; Ogunlaja, A. S., Nanomaterials as catalysts for CO_2 transformation into value-added products: A review. *Sci Total Enviro.* **2023,** 868, 161547.
2. Zhao, M.; Gu, Y.; Gao, W.; Cui, P.; Tang, H.; Wei, X.; Zhu, H.; Li, G.; Yan, S.; Zhang, X.; Zou, Z., Atom vacancies induced electron-rich surface of ultrathin Bi nanosheet for efficient electrochemical CO_2 reduction. *Appl. Catal. B: Environ.* **2020,** 266, 118625.
3. Feng, X.; Zou, H.; Zheng, R.; Wei, W.; Wang, R.; Zou, W.; Lim, G.; Hong, J.; Duan, L.; Chen, H., Bi_2O_3/BiO_2 Nanoheterojunction for Highly Efficient Electrocatalytic CO_2 Reduction to Formate. *Nano Lett.* **2022,** 22, (4), 1656-1664.
4. Yang, Y.; He, A.; Yang, M.; Zou, Q.; Li, H.; Liu, Z.; Tao, C.; Du, J., Selective electroreduction of CO_2 to ethanol over a highly stable catalyst derived from polyaniline/$CuBi_2O_4$. *Catalysis Science & Technology.* **2021,** 11, (17), 5908-5916.
5. Sakamoto, N.; Nishimura, Y. F.; Nonaka, T.; Ohashi, M.; Ishida, N.; Kitazumi, K.; Kato, Y.; Sekizawa, K.; Morikawa, T.; Arai, T., Self-assembled Cuprous Coordination Polymer as a Catalyst for CO_2 Electrochemical Reduction into C2 Products. *ACS Catal.* **2020,** 10, (18), 10412-10419.
6. Liu, B.; Yao, X.; Zhang, Z.; Li, C.; Zhang, J.; Wang, P.; Zhao, J.; Guo, Y.; Sun, J.; Zhao, C., Synthesis of Cu_2O Nanostructures with Tunable Crystal Facets for Electrochemical CO_2 Reduction to Alcohols. *ACS Appl Mater Interfaces.* **2021,** 13, (33), 39165-39177.
7. Zhou, X.; Shan, J.; Chen, L.; Xia, B. Y.; Ling, T.; Duan, J.; Jiao, Y.; Zheng, Y.; Qiao, S. Z., Stabilizing Cu^{2+} Ions by Solid Solutions to Promote CO_2 Electroreduction to Methane. *J Am Chem Soc.* **2022,** 144, (5), 2079-2084.
8. Dong, W.; Zhang, N.; Li, S.; Min, S.; Peng, J.; Liu, W.; Zhan, D.; Bai, H., A Mn single atom catalyst with Mn–N_2O_2 sites integrated into carbon nanosheets for efficient electrocatalytic CO_2 reduction. *J Mater Cheme A.* **2022,** 10, (20), 10892-10901.
9. Clark, E. L.; Ringe, S.; Tang, M.; Walton, A.; Hahn, C.; Jaramillo, T. F.; Chan, K.; Bell, A. Influence of Atomic Surface Structure on the Activity of Ag for the Electrochemical Reduction of CO_2 to CO. *ACS Catal.* **2019,** 9, (5), 4006-4014.
10. Wang, Q.; Liu, K.; Hu, K.; Cai, C.; Li, H.; Li, H.; Herran, M.; Lu, Y.-R.; Chan, T.-S.; Ma, C. J. Attenuating metal-substrate conjugation in atomically dispersed nickel catalysts for electroreduction of CO_2 to CO. *Nat Commun.* **2022,** 13, (1), 6082.
11. Duan, Y. X.; Zhou, Y. T.; Yu, Z.; Liu, D. X.; Wen, Z.; Yan, J. M.; Jiang, Q. J. Boosting production of HCOOH from CO_2 electroreduction via Bi/CeOx. *Angew Chem Int Ed Engl.* **2021,** 60, (16), 8798-8802.
12. Koh, J. H.; Won, D. H.; Eom, T.; Kim, N.-K.; Jung, K. D.; Kim, H.; Hwang, Y. J.; Min, B. K. Facile CO_2 electro-reduction to formate via oxygen bidentate intermediate stabilized by high-index planes of Bi dendrite catalyst. *ACS Catal.* **2017,** 7, (8), 5071-5077.
13. Li, D.; Huang, L.; Tian, Y.; Liu, T.; Zhen, L.; Feng, Y. Facile synthesis of porous Cu-Sn alloy electrode with prior selectivity of formate in a wide potential range for CO_2 electrochemical reduction. *Appl. Catal. B Environ.* **2021,** 292, 120119.
14. Grace, A. N.; Choi, S. Y.; Vinoba, M.; Bhagiyalakshmi, M.; Chu, D. H.; Yoon, Y.; Nam, S. C.; Jeong, S. K. Electrochemical reduction of carbon dioxide at low overpotential on a polyaniline/Cu_2O nanocomposite based electrode. *Applied Energy.* **2014,** 120, 85-94.

15. Boutin, E.; Wang, M.; Lin, J. C.; Mesnage, M.; Mendoza, D.; Lassalle-Kaiser, B.; Hahn, C.; Jaramillo, T. F.; Robert, M. J. A. C. I. E., Aqueous electrochemical reduction of carbon dioxide and carbon monoxide into methanol with cobalt phthalocyanine. *Angew.Chem.Int.Ed.* **2019,** 58, (45), 16172-16176.
16. Ren, D.; Deng, Y.; Handoko, A. D.; Chen, C. S.; Malkhandi, S.; Yeo, B. S. J. Selective electrochemical reduction of carbon dioxide to ethylene and ethanol on copper (I) oxide catalysts. *ACS Catal.* **2015,** 5, (5), 2814-2821.
17. Yuan, J.; Yang, M.-P.; Zhi, W.-Y.; Wang, H.; Wang, H.; Lu, J.-X. Efficient electrochemical reduction of CO_2 to ethanol on Cu nanoparticles decorated on N-doped graphene oxide catalysts. *J. CO_2 Util.* **2019,** 33, 452-460.
18. Iyengar, P.; Huang, J.; De Gregorio, G. L.; Gadiyar, C.; Buonsanti, R. Size dependent selectivity of Cu nano-octahedra catalysts for the electrochemical reduction of CO_2 to CH_4. *Chem Commun (Camb).* **2019,** 55, (60), 8796-8799.
19. Chu, S.; Kang, C.; Park, W.; Han, Y.; Hong, S.; Hao, L.; Zhang, H.; Lo, T. W. B.; Robertson, A. W.; Jung, Y.; Han, B.; Sun, Z. Single atom and defect engineering of CuO for efficient electrochemical reduction of $CO_2$to C_2H_4. *SmartMat.* **2022,** 3, (1), 194-205.
20. Luo, H.; Li, B.; Ma, J. G.; Cheng, P., Surface Modification of Nano-Cu_2 O for Controlling CO_2 Electrochemical Reduction to Ethylene and Syngas. *Angew Chem Int Ed Engl.* **2022,** 61, (11), e202116736.
21. Tan, X.; Yu, C.; Zhao, C.; Huang, H.; Yao, X.; Han, X.; Guo, W.; Cui, S.; Huang, H.; Qiu, J. J. Interfaces, Restructuring of Cu_2O to Cu_2O@ Cu-metal–organic frameworks for selective electrochemical reduction of CO_2. *ACS Appl. Mater. Interfaces.* **2019,** 11, (10), 9904-9910.
22. Cao, S.; Chen, H.; Han, T.; Zhao, C.; Peng, L. J. Rose-like Cu_2O nanoflowers via hydrothermal synthesis and their gas sensing properties. *Materials Lett.* **2016,** 180, 135-139.
23. Gao, Y.; Wu, Q.; Liang, X.; Wang, Z.; Zheng, Z.; Wang, P.; Liu, Y.; Dai, Y.; Whangbo, M. H.; Huang, B., Cu_2O Nanoparticles with Both 100 and 111 Facets for Enhancing the Selectivity and Activity of CO_2 Electroreduction to Ethylene. *Adv Sci (Weinh)* **2020,** 7, (6), 1902820.
24. Fu, W.; Liu, Z.; Wang, T.; Liang, J.; Duan, S.; Xie, L.; Han, J.; Li, Q. J. Engineering, Promoting C2+ production from electrochemical CO_2 reduction on shape-controlled cuprous oxide nanocrystals with high-index facets. *ACS Sustainable Chem. Eng.***2020,** 8, (40), 15223-15229.
25. Luo, T.; Liu, K.; Fu, J.; Chen, S.; Li, H.; Hu, J.; Liu, M. J. Tandem catalysis on adjacent active motifs of copper grain boundary for efficient CO_2 electroreduction toward C2 products. *Journal of Energy Chemistry* **2022,** 70, 219-223.
26. Wang, Y.; Lou, Z.; Niu, W.; Ye, Z.; Zhu, L. J. Optimization of photoelectrochemical performance in Pt-modified p-Cu_2O/n-Cu_2O nanocomposite. *Nanotechnology* **2018,** 29, (14), 145402.
27. Feng, Y.; Li, Z.; Liu, H.; Dong, C.; Wang, J.; Kulinich, S. A.; Du, X. J. Laser-prepared CuZn alloy catalyst for selective electrochemical reduction of CO_2 to ethylene. *Langmuir* **2018,** 34, (45), 13544-13549.
28. Chen, C.; Sun, X.; Yan, X.; Wu, Y.; Liu, M.; Liu, S.; Zhao, Z.; Han, B. J. G. strategy to control the grain boundary density and Cu^+/Cu^0 ratio of Cu-based catalysts for efficient electroreduction of CO_2 to C2 products. *Green Chem.* **2020,** 22, (5), 1572-1576.
29. Luo, H.; Li, B.; Ma, J. G.; Cheng, P. J. Surface Modification of Nano-Cu_2O for Controlling CO_2 Electrochemical Reduction to Ethylene and Syngas. *Angew Chemie.* **2022,** 134, (11), e202116736.
30. Shang, L.; Lv, X.; Shen, H.; Shao, Z.; Zheng, G., Selective carbon dioxide electroreduction to ethylene and ethanol by core-shell copper/cuprous oxide. *J Colloid Interface Sci.* **2019,** 552, 426-431.
31. Ning, H.; Wang, X.; Wang, W.; Mao, Q.; Yang, Z.; Zhao, Q.; Song, Y.; Wu, M., Cubic Cu2O on nitrogen-doped carbon shells for electrocatalytic CO2 reduction to C_2H_4. *Carbon* **2019,** 146, 218-223.
32. Chang, X.; Wang, T.; Zhao, Z. J.; Yang, P.; Greeley, J.; Mu, R.; Zhang, G.; Gong, Z.; Luo, Z.; Chen, J. J. Tuning Cu/Cu_2O interfaces for the reduction of carbon dioxide to methanol in aqueous solutions. *Angew.Chem.Int.E.* **2018,** 57, (47), 15415-15419.
33. Qiu, Y.-L.; Zhong, H.-X.; Zhang, T.-T.; Xu, W.-B.; Li, X.-F.; Zhang, H.-M. Copper Electrode Fabricated via Pulse Electrodeposition: Toward High Methane Selectivity and Activity for CO_2 Electroreduction. *ACS Catal.* **2017,** 7, (9), 6302-6310.
34. Zheng, Y.; Zhang, L.; Guan, J.; Qian, S.; Zhang, Z.; Ngaw, C. K.; Wan, S.; Wang, S.; Lin, J.; Wang, Y. J. Engineering, Controlled synthesis of Cu^0/Cu_2O for efficient photothermal catalytic conversion of CO_2 and H_2O. *ACS Sustainable Chem. Eng.* **2021,** 9, (4), 1754-1761.
35. Wang, S.; Kou, T.; Varley, J. B.; Akhade, S. A.; Weitzner, S. E.; Baker, S. E.; Duoss, E. B.; Li, Y. J. Cu_2O/CuS nanocomposites show excellent selectivity and stability for formate generation via electrochemical reduction of carbon dioxide. *ACS Materials Lett.* **2020,** 3, (1), 100-109.
36. Lv, X.-W.; Liu, Y.; Hao, R.; Tian, W.; Yuan, Z.-Y. Urchin-like Al-doped Co_3O_4 nanospheres rich in surface oxygen vacancies enable efficient ammonia electrosynthesis. ACS Appl. *Mater. Interfaces.* **2020,** 12, (15), 17502-17508.

37. Sun, B.; Dai, M.; Cai, S.; Cheng, H.; Song, K.; Yu, Y.; Hu, H. J. Challenges and strategies towards copper-based catalysts for enhanced electrochemical CO_2 reduction to multi-carbon products. *Fuel* **2023,** 332, 126114.
38. Li, Y. C.; Wang, Z.; Yuan, T.; Nam, D.-H.; Luo, M.; Wicks, J.; Chen, B.; Li, J.; Li, F.; De Arquer, F. P. G. Binding site diversity promotes CO_2 electroreduction to ethanol. *J Am Chem Soc***. 2019,** 141, (21), 8584-8591.
39. Yang, R.; Wu, Z.; Tang, D.; Xing, Y.; Ren, Y.; Li, F.; Li, X., Synthesis of Cu_2O crystals with negative surface curvature at various positions via Al^{3+} ions inducing. *Materials Lett.* **2014,** 117, 211-213.